# Sputtered lead scandium tantalate thin films: a microstructural study

Z. HUANG*
*Department of Physics, University of Essex, Colchester CO4 3SQ, UK*

M. A. TODD, R. WATTON
*DRA, St. Andrews Rd, Great Malvern, Worcs, WR14 3PS, UK*

R. W. WHATMORE
*School of Industrial and Manufacturing Science, Cranfield University, Cranfield, Bedford, MK43 0AL, UK*

Lead scandium tantalate (PST) thin films have been deposited on a platinized silicon substrate with and without a buffer layer of MgO at the temperature of 525 °C. It was found that PST films on the substrate without a buffer layer were strongly (1 1 1) oriented perovskite, whilst films on the substrate with a buffer layer showed the presence of second-phase pyrochlore, and the films were (1 1 1) and (1 1 0) oriented. These structural differences were believed to result from the structural differences between the platinum layers immediately below the respective PST layers. The ''lines'' which divide PST into ''network'' of islands were found to be no more than wider grain boundaries, rather than ''cracks'' as believed previously. Micro-beam diffraction and energy dispersive X-ray analysis showed that grain boundaries were tantalum-rich and lead-deficient compared to perovskite grain centres. Electrical properties, such as relative permittivity and dielectric loss, for the films were also measured.

## 1. Introduction

In recent years there has been considerable interest in the development of materials to be used in pyroelectric infrared detection and thermal imaging [1]. Amongst the candidates is lead scandium tantalate, $Pb(Sc_{1/2}Ta_{1/2})O_3$ (PST). PST is a ferroelectric "relaxor" oxide with a ferroelectric Curie temperature between 0 and 26 °C [2–7]. Above the Curie temperature, it has a structure similar to cubic perovskite, and conforms to the general formula, $AB'_{1/2}B''_{1/2}O_3$. The annealing of PST results in the ordering of scandium and tantalum cations on alternate $\{1\,1\,1\}$ planes, leading to the formation of a face-centred cubic superlattice [8, 9]. This produces reflections at the positions of $\{h + 1/2,\ k + 1/2,\ l + 1/2\}$ in X-ray and electron diffraction patterns.

Due to the need for miniaturization and compatibility with silicon-integrated circuit fabrication, techniques have been developed to deposit PST as thin films directly on to a given substrate [10]. Several methods have been employed for this purpose, including reactive sputtering [11, 12], sol–gel coating [13, 14] and pulsed-laser deposition [15]. A major practical problem for PST has been the high annealing temperatures ( > 900 °C) needed for the crystallization of films to the desired perovskite phase [11, 14]. However, it has been shown that perovskite-structured PST thin films can be directly deposited on sapphire coated with MgO, in a much lower temperature range of 500–550 °C by means of reactive sputtering, with a large excess lead [10]. In the present study, PST films prepared by reactive sputtering on platinum and MgO-coated silicon, were characterized by microstructural and electrical studies.

## 2. Experimental procedure

Two substrate configurations were used in this study. In the first, thermally oxidized silicon ($SiO_2$/Si) was coated with titanium and platinum (Pt/Ti) by electron-beam evaporation, with the titanium acting as an adhesion layer for the platinum. In the second configuration, a further layer of thin-film magnesium oxide (MgO) was added by diode sputtering, which was coated with another platinum/titanium layer. These substrates were used for PST film deposition. The PST was deposited by reactive magnetron sputtering from a composite metal target in an argon/10% oxygen atmosphere in a Nordiko 2000 sputterer. The sputtering target consisted of alternate sectors of scandium

* *Present address*: School of Industrial and Manufacturing Science, Cranfield University, Cranfield Bedford, MK43 0AL, UK, to which all correspondence should be addressed.

0022–2461 

and tantalum with lead pellets placed on top. These pellets were replaced for each deposition. The deposition conditions were set to give a Ta:Sc ratio around 1:1, whilst the lead ratio could be varied from Pb:Sc 1.5:1 to 3.5:1 by adjusting the size, number and position of the pellets. (The stoichiometric PST ratio Pb:Sc:Ta is 2:1:1). The substrate temperature during PST deposition was limited to 525 °C to ensure compatibility with active silicon circuitry (although plain silicon wafers were used in these trials). No post-deposition annealing was performed.

The two samples studied were labelled CH385 and CH445. CH385 had the structure PST/Pt/Ti/$SiO_2$/Si with the respective film thicknesses 1.0 μm/150 nm/5 nm/0.8 μm/500 μm. CH445 included a 1 μm thick MgO underlayer and had the structure PST/Pt/Ti/ MgO/Pt/Ti/$SiO_2$/Si with the respective film thicknesses 1.1 μm/90 nm/5 nm/1.0 μm/200 nm/50 nm/0.8 μm/500 μm.

For cross-section TEM sample preparation, the films with the substrate were cut into strips of $\sim 5\,\text{mm} \times 3\,\text{mm}$. These were glued together with the films face-to-face, and the glued stack was inserted into a spring-loaded clamp to make the glue bond as thin and as uniform as possible. Mechanical grinding and polishing were used to reduce the thicknesses of samples to 20–30 μm for cross-section samples and 10–20 μm for plan-view samples. Each sample was ion-beam thinned, operating at 5 kV, at an incident angle of 20° initially and 15°–12° in the later stages. Cross-sectional TEM samples were thinned from both sides while plan-view samples were thinned from the silicon side only. To obtain a plan-view of the MgO alone, the sample was first thinned from the PST film side to remove the PST film and the underlying platinum and titanium layers and then it was thinned from the silicon side until electron transparent. TEM observation was carried out on Jeol 200CX and Topcon 002B microscopes, operating at 200 kV. Both were equipped with Link EDX systems. SEM observation was performed on Cambridge S360. X-ray diffraction investigation was carried out on a Phillips PW1710 diffractometer, with Cu$k_\partial$ as the X-ray radiation.

Additional substrate pieces were used to measure electrical properties. 1.5 mm diameter nichrome electrodes were thermally evaporated through a shadow mask on to the PST films. One contact was made to the underlying platinum whilst the other, spring-loaded, contact was made to the individual nichrome electrodes. Measurements were made of capacitance and dielectric loss against temperature using a Wayne-Kerr 6425 Component Analyser. From the capacitance results, the relative permittivity was calculated using a simple parallel plate capacitor model.

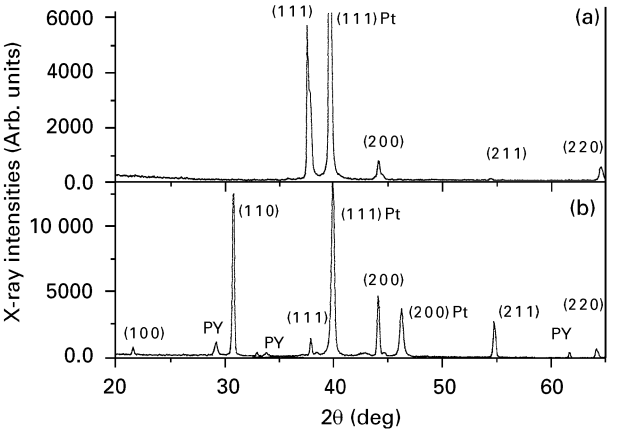


*Figure 1* X-ray diffraction patterns for PST films: (a) CH385, (b) CH445.

## 3. Results

### 3.1. X-ray diffraction

Fig. 1 shows θ/2θ scan X-ray diffraction patterns for CH385 PST on (a) Pt/Ti/$SiO_2$/Si and (b) CH445 PST on Pt/Ti/MgO/Pt/Ti/$SiO_2$/Si. Apart from the indicated platinum and PY (for pyrochlore) peaks, all others are perovskite. The indices were based on the ideal cubic perovskite phase. It can be seen that for CH385, the Pt was (1 1 1) oriented. The PST was strongly (1 1 1) preferentially oriented. There is no peak from pyrochlore phase. However, a peak-splitting was observed for the PST (1 1 1) peak, and further investigations also found peak-splitting for the PST (2 2 2). Two explanations could be suggested for this phenomenon: either the PST was actually in the rhombohedral state or there were two cubic phases with slightly different lattice parameters in the film. The detailed study of this is a subject for a separate publication. For sample CH445, the platinum electrode was no longer solely (1 1 1) oriented; (2 0 0) Pt was also observed. For PST, apart from perovskite diffraction lines, there were also pyrochlore peaks as labelled by PY in the pattern. (1 1 0), rather than (1 1 1), is the preferred orientation for the perovskite PST. The lattice diameters were surprisingly large for the film CH445: $a_0 = 0.4111$ nm compared with $a_0 = 0.407$ nm for bulk ceramic material [16]. Possible reasons for this are discussed in an associate paper [17]. The electrode platinum ($a_0 = 0.392\,31$ nm) was used as an *in situ* standard for the calculation of *d*-spacing. The lattice parameter for the CH385 was not calculated because of the peak-splitting noted above. The lattice parameter so determined for the pyrochlore is $a_0 = 1.060$ nm. Because the first platinum layer (the platinum layer before MgO was deposited) was deposited in the same way as that for CH385, it should be highly (1 1 1) oriented, as in CH385. This implies that the (2 0 0) Pt must exist in the second (upper) platinum layer, which was prepared after the MgO layer was deposited. This (2 0 0) oriented platinum bottom electrode in turn affected the growth of the perovskite phase in the PST.

### 3.2. SEM results

Fig. 2 shows SEM images of (a) secondary electron (SE) image for CH385, (b) back-scattering electron (BS) image for CH385, and (c) BS image for CH445. The SE image shows PST surface in CH385 as being rather uniform, with grain size at about 0.1 μm. The two BS images clearly show "lines" in the two films. In

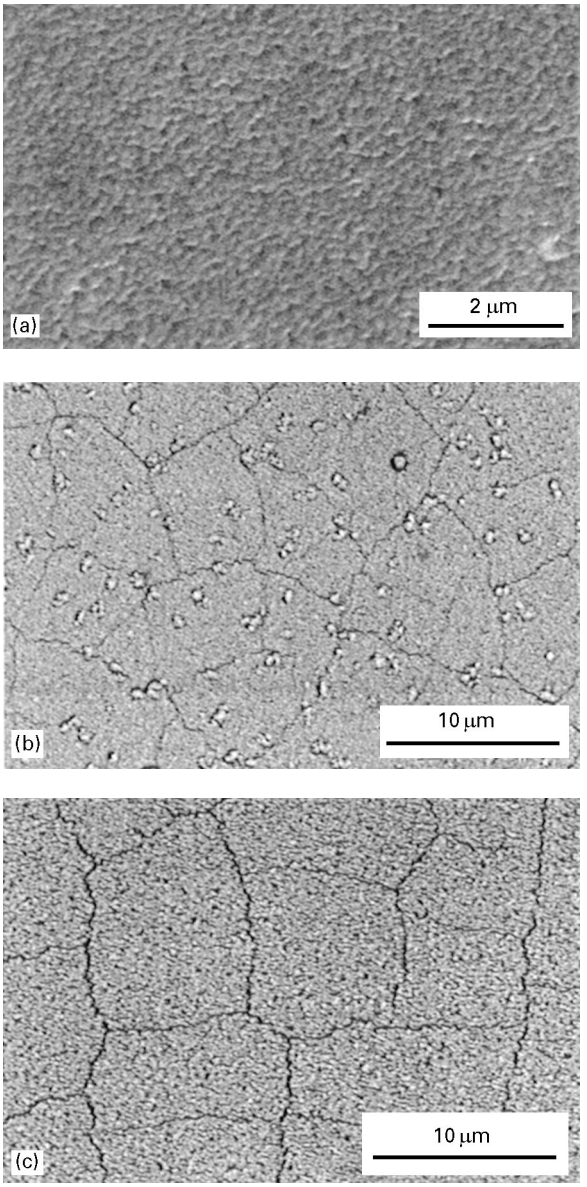


*Figure 2* SEM images: (a) secondary electron image for PST CH385, (b) back-scattering electron image for CH385, (c) back-scattering electron image for CH445. "Lines" can be readily seen in the back-scattering images whilst they are not clear in the secondary image. Network of "lines" dividing the PST into islands.

fact, a "network" of these lines existed all over the films, dividing the PST into large, roughly square islands around 5 μm × 5 μm for CH385 and 8 μm × 8 μm for CH445 in size, respectively.

Fig. 3 shows (a) SE and (b) BS images for CH445. The SE and BS images were taken from exactly the same position. Here, the PST grains were larger, up to 0.5 μm in diameter, and grain facets and grain boundaries can readily be seen. The film was concave at the centre of the "line" which was 0.1–0.5 μm wide as seen from the SE image (a). The BS image (b) from the same area shows grains existing at the position of the line in the SE image, as indicated by arrow heads in the pictures. The grain boundaries and line centres showed the same contrast relative to the grains in the BS image, indicating that they are probably of the same nature in chemical composition and crystallization. These lines, therefore, do not appear to be

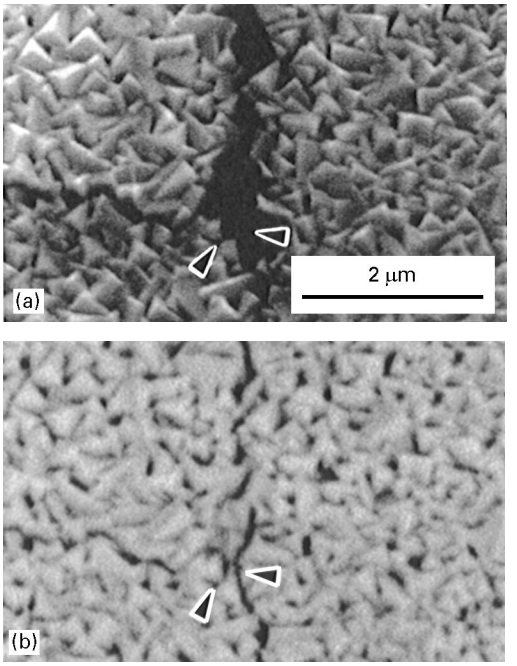


*Figure 3* SEM images for PST CH445: (a) secondary electron mode, (b) back-scattering mode. The surface of PST was concave at the positions of the "lines".

cracks– as usually believed – but more likely a regular coalescence of the same material which appears at the grain boundaries.

### 3.3. TEM results

Plan-view TEM observations showed that the PST grain size for CH385 was 0.1–0.5 μm, in agreement with the SEM results. Micro-beam diffraction (MBD) showed that almost every grain was in the (1 1 1) orientation, in agreement with the X-ray diffraction observations. It was also observed that the grain boundaries were amorphous. Fig. 4 shows a plan-view image for CH385. The inset is a MBD pattern for the dark grain in the top left of the photograph, which can be indexed as the (1 1 1) pattern of perovskite PST. All three grains in the picture showed the (1 1 0) lattice image. Amorphous regions at grain boundaries can be recognized. Fig. 5 shows a picture of a grain boundary after the area was illuminated twice by the electron beam. The areas hit by the electron beam can readily be recognized, and were marked as A and B in the picture. Area A was used for EDX analysis, illuminated for a period of 100 s. Area B was illuminated for a few seconds, to obtain an MBD pattern. The MBD pattern (inset) in the picture showed a faint ring (marked by arrow heads) which can be indexed to the (4 4 4) of the pyrochlore. Lattice images, e.g. (2 2 2) lattice of 0.31 nm, can be seen at various parts of the image, as indicated by small arrow heads. This suggests that the amorphous material at the grain boundary was transformed to pyrochlore by the strong electron-beam illumination.

A plan-view TEM image for CH445 is shown in Fig. 6a. The PST grain size was up to 0.5 μm, again confirming the SEM results. By using MBD, PST grains were found mainly oriented in the (1 1 1) and

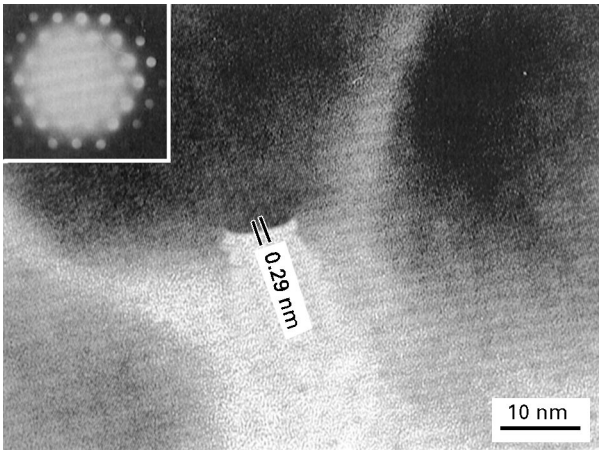


*Figure 4* TEM image for plan-view PST CH385. The inserted MBD pattern corresponds to (1 1 1) perovskite PST. All the grains were (1 1 1) oriented. Grain boundaries were amorphous.

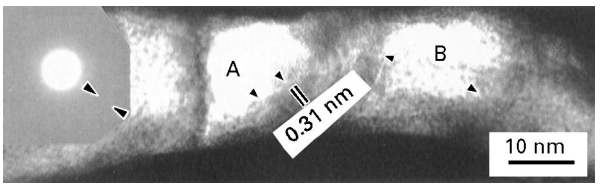


*Figure 5* High-resolution transmission electron micrograph of a grain boundary for PST CH385 after the area was hit by electron beams. The areas A and B, hit by the electron beam, can readily be seen. The MBD (the inset) shows the area was transformed into pyrochlore. Lattice images marked by small arrow heads also show the grain boundary was no longer amorphous after the illumination with the strong electron beam.

(1 1 0) directions. Fig. 6b and c show diffraction patterns from different grains, whilst Fig. 6d shows a typical diffraction pattern from grain boundaries and "line" centres, as indicated by the thin arrows on the figure. When a beam was positioned to include both grain and grain boundary, a superimposed diffraction pattern was obtained (the inset). This diffraction pattern shows that the (1 1 0) spots of perovskite are at the outer-part of the first ring, indicating the *d*-value for the ring is larger than the 0.29 nm for the (1 1 0) perovskite, and ruling out the possibility that the ring diffraction comes from a PbO phase, as has been suggested previously [18]. A "line" position is marked by wide arrows in the picture. The line centre showed the same diffraction pattern as a grain boundary. The first (0.31 nm) and the faint second (0.15 nm) rings were indexed as pyrochlore (2 2 2) and (4 4 4) (Fig. 6d). This is in agreement with the X-ray diffraction results indicating that a pyrochlore phase existed together with the perovskite. No superlattice diffraction was observed, indicating that no B cation ordering has taken place. This is not surprising, because the temperature (525 °C) used in the preparation of the thin films was far below the minimum temperature (600 °C) needed to cause lattice ordering in this system [14]. EDX results from a grain boundary (e) and the grain centre adjacent to this boundary (f) show that the boundary was tantalum-rich compared to the grain centre. The Sc/Pb ratios were very close for grain boundary and grain centre, but Ta/Pb ratio for the grain boundary was far larger than that for the grain centre. This was proved to be true also for other grain boundaries and the respective adjacent grain centres [17].

Fig. 7 shows a high-resolution image for sample CH445. It can be seen that at the centre of the grain boundary, A, it is still amorphous. However, the grains B and C seem not as well crystallized as those in CH385. Micro-crystals still exist at the edge of the crystal grain (marked by arrow heads in the picture). It is considered that these could be pyrochlore crystallites that were not yet transformed into perovskite. The evidence for this is the existence of pyrochlore as detected by MBD (inset in Fig. 6a). It can be seen clearly that this phase is not present at the centres of grain boundaries, nor the centres of the perovskite grains. Hence the strong likelihood is that the microcrystallites indicated are the pyrochlore phase.

A plan-view image for MgO is shown in Fig. 8a. The MgO was highly textured around [0 0 1]. A MBD for one crystal and selected-area diffraction pattern for many crystals were shown in Fig. 8b and c, respectively. The MBD showed the (0 0 1) pattern for single-crystal MgO. The MgO grain size was about 0.1 μm. The uniform intensity within one ring of the selected-area diffraction pattern suggests that there was no preferred orientation in the plane perpendicular to the [0 0 1] direction.

Fig. 9 shows a cross-section TEM image for CH385. Columnar PST grains were evident. The cross-section image for CH445 is shown in Fig. 10, (a) $Si/SiO_2/Pt/MgO$ (from left to right), (b) Pt/PST. The diameter of columnar PST grains were clearly larger in Fig. 10b than in Fig. 9, as expected from plan-view observation. The columnar PST started from the PST/Pt interface and in most cases continued to the surface of the film.

### 3.4. Electrical results

Fig. 11 shows the relative permittivity against temperature graphs for CH385 and CH445, both measured at three frequencies, i.e. 120, 1500 Hz and 10 kHz. Fig. 12 is a plot of the dielectric loss, or loss tangent against temperature for the same frequencies. The dispersion shown on the CH385 results may be due to the fact that this film had a low, temperature-dependent d.c. electrical resistivity ($2 \times 10^9$ Ωm at 36 °C). The resistivity of CH445 was measured as $6 \times 10^{11}$ Ωm and the observed dielectric results are more typical of the results obtained on these high-lead, low deposition temperature PST films. The permittivity of CH445 films falls with increasing temperature over this range, indicating a peak in permittivity below 0 °C. This is in contrast to ordered bulk ceramic PST where the peak permittivity occurs around 10–20 °C, though it has been shown that the peak moves to lower temperature with less-ordered material [9].

When used for infrared detection, PST is used in a dielectric bolometer mode where the pyroelectricity is induced by a d.c. bias field. Induced pyroelectric coefficient measurements have been made on CH445

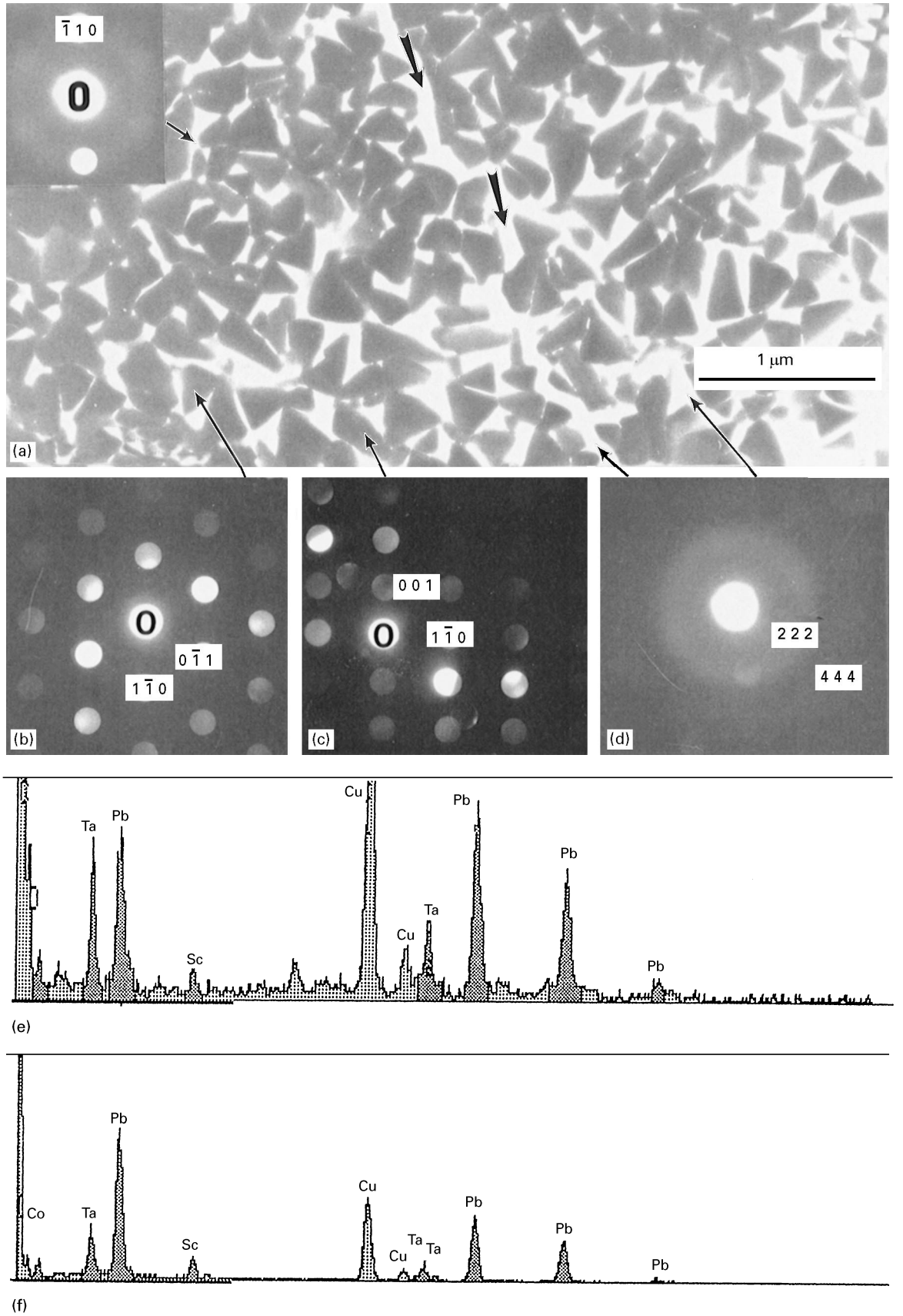


*Figure 6* TEM pictures for PST CH445: (a) plan-view image. Micro-beam diffraction patterns show different grains were at different orientations: (b) (1 1 1) pattern, (c) (1 1 0) pattern. Grain boundary and "line" centre were pyrochlore (d). EDX spectra were shown in (e) for a grain boundary, and (f) for a grain centre.

using a low-frequency a.c. temperature stimulation. The results for an average temperature of 39 °C are shown in Fig. 13. The pyroelectric coefficient increases with increasing bias up to 7 V $\mu m^{-1}$. Induced pyroelectric measurements could not be made on CH385, due to leakage current effects.

These measurements imply that CH445 has better ferroelectric properties than CH385 and that CH385

suffers additionally from a low resistivity, which would make it of little use for IR imaging. The pyroelectric properties of CH445 are much reduced compared with bulk PST and about half that of the best PST films deposited at silicon-compatible temperatures [19]. However, when deposited on low thermal conductance microbridges, films of this nature would give adequate infrared imaging performance for a number of applications.

## 4. Discussion

It is widely suggested [20] that in many processes such as sol–gel for PZT, the crystallization of perovskite occurs by the following path: from amorphous to pyrochlore to perovskite. Our TEM investigation suggests that this may also be the favoured route for the transformation to perovskite in the directly sputtered PST, because the amorphous material in the grain boundaries was transformed to pyrochlore by the strong electron beam. It is not clear whether this transformation was induced by the electron-beam heating or electric field or both.

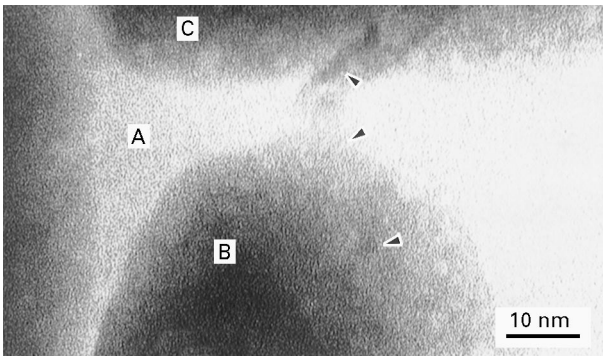


*Figure 7* High-resolution TEM picture for PST CH445. Grain boundary A is amorphous, grains B and C were perovskite, and pyrochlore crystals (marked by arrow heads) were at the edge of grains to grain boundaries.

X-ray and TEM experiments have found substantial differences for PST films CH385 and CH445, in terms of the presence of second-phase pyrochlore, perovskite PST grain size and preferred orientations. Both films were deposited by direct sputtering on to a bottom electrode platinum. The only difference was that for CH385, the PST was deposited on to the platinized substrate $Pt/Ti/SiO_2/Si$ directly, whilst for CH445 an additional layer of Pt/Ti/MgO was coated on to the platinized substrate before the PST was sputtered on. Therefore, it is reasonable to suggest that the PST structure difference resulted from this Pt/Ti/MgO layer. The (2 0 0) oriented platinum indicated by X-ray diffraction in the upper platinum layer is presented for the same reason. Therefore, the orientation of the platinum layer immediately beneath the PST for CH445 is quite different from that for CH385, which was exclusively (1 1 1) oriented. It is believed that the (1 1 1) orientation of PZT thin films reported elsewhere results from the crystallographic match of PZT (1 1 1) to Pt (1 1 1) [20, 21]. It is also suggested that nanocrystalline pyrochlore PZT will more readily transform to perovskite on (1 1 1)

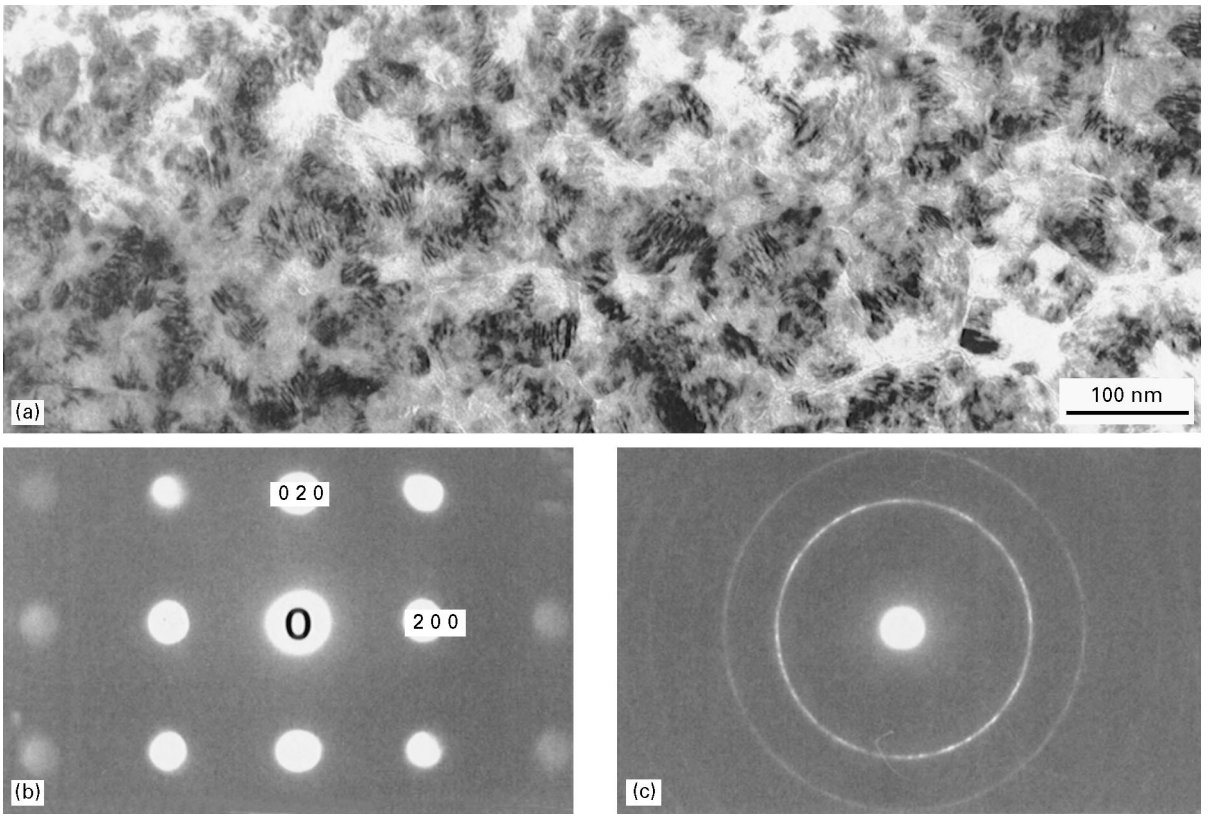


*Figure 8* TEM pictures for MgO layer in CH445: (a) plan-view image, (b) micro-beam diffraction pattern of (0 0 1) from one crystal, (c) selected-area diffraction pattern for many crystals. The MgO was textured at the (0 0 1) direction.

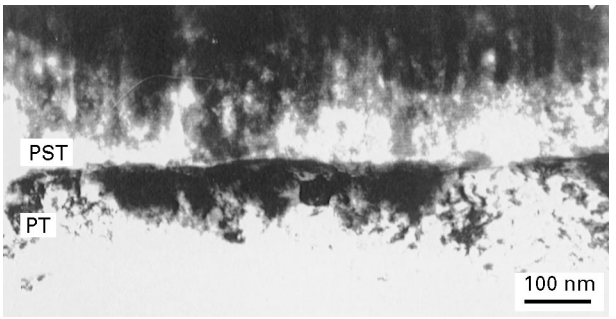


*Figure 9* TEM cross-section image for CH385 shows a high-quality interface of PST/Pt and columnar PST grains in the thin film.

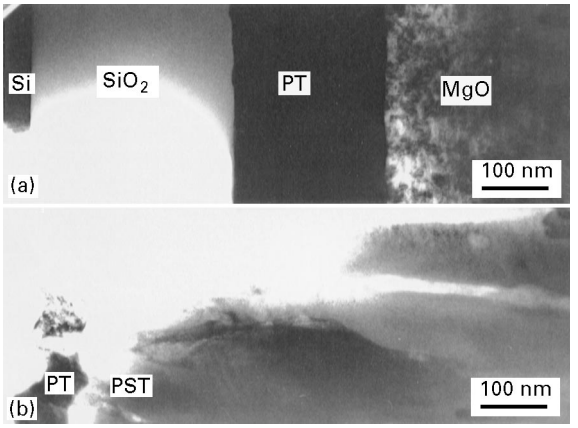


*Figure 10* TEM cross-section images for CH445: (a) MgO/Pt/$SiO_2$/Si, (b) PST/MgO. Columnar PST grains and their grain boundaries can be seen clearly in (b).

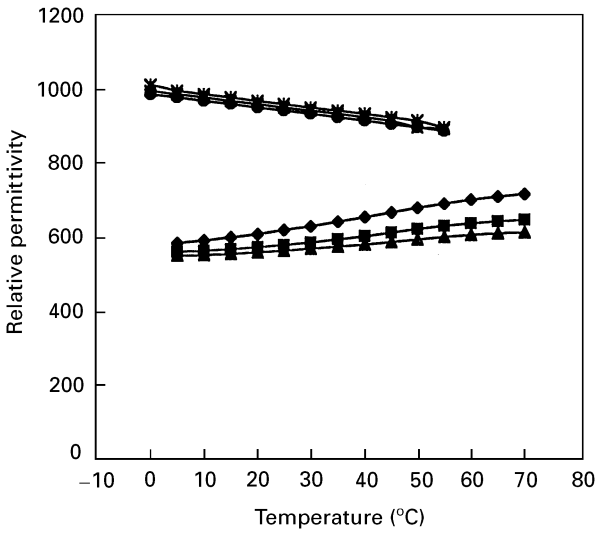


*Figure 11* Relative permittivity plotted against temperature for PST films (◆, ■, ▲) CH385 and (✱, ×, ●) CH445. (◆, ✱) 120 Hz, (■, ×) 1500 Hz, (▲, ●) 10 kHz.

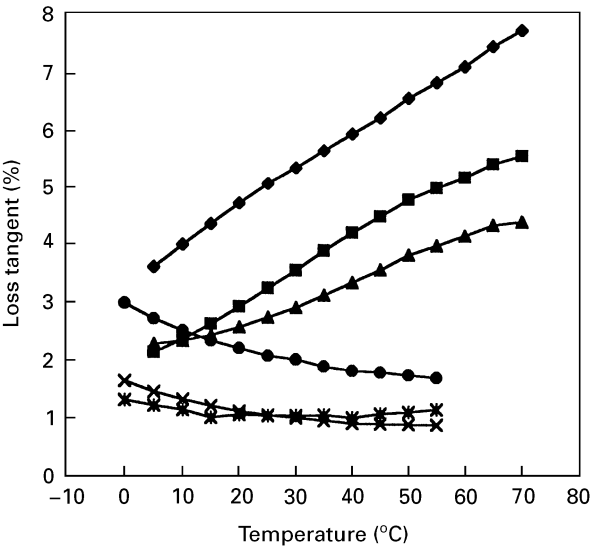


*Figure 12* Loss tangent against temperature for PST films (◆, ■, ▲) CH385 and (✱, ×, ●) CH445. (◆, ✱) 120 Hz, (■, ×) 1500 Hz, (▲, ●) 10 kHz.

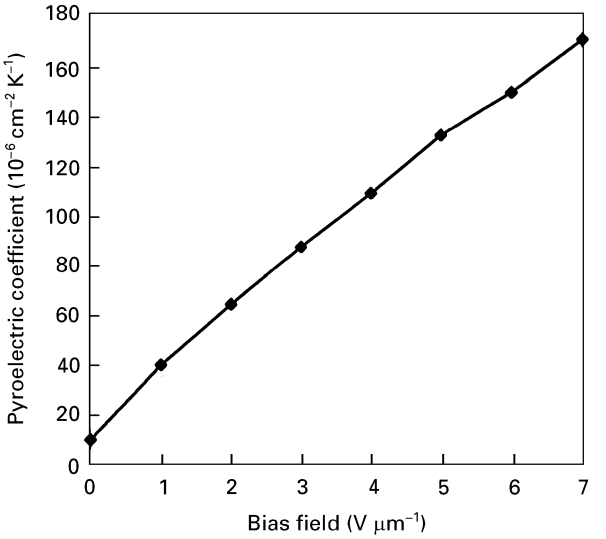


*Figure 13* Pyroelectric coefficient against bias field for the PST film CH445.

oriented nuclei than on other orientations such as (1 0 0) [20]. If this is also true for PST, it is not difficult to understand the differences between CH385 and CH445. All the nuclei in CH385 were (1 1 1) and thus would more easily convert the pyrochlore matrix to perovskite than CH445, because in the latter film, beside (1 1 1) nuclei there were also (2 0 0) ones which were more resistant to transform to perovskite. However, the electrical properties, such as relative permittivity and dielectric loss, for CH385 were worse than those for CH445, despite the fact that a pyrochlore second phase was observed in CH445 whilst no pyrochlore existed in CH385. The permittivity and loss tangent properties as a function of temperature were also different for the two films; e.g. with increasing temperature the permittivity falls for the films CH445 but increases for the films CH385. These may be related to the XRD peak-splitting for the films CH385. Further study of this is in progress.

The lattice parameter for PST is normally $a_0 = 0.407$ nm [16]. Lattice parameters for our PST films were unusually large compared with this value. It

is believed this may due to $Pb^{4+}$ cation occupying B positions in the perovskite structure. This assumption can also explain the large excess of lead (30%) present in the film. A separate publication will deal with this in detail [17].

At first sight, the "network" of lines in Fig. 2 could easily be assumed as being a "crack network", formed because of the volume shrinkage during the transformation from pyrochlore to perovskite. However, both our SEM and TEM observations have demonstrated that these lines were no more than wider grain boundaries. The PST is concave along these lines but there are perovskite grains within the concave area. This implies that these "lines" were formed during the growth process rather than in the transformation process, otherwise there would be no material at the position of "lines" and they would then be genuine "cracks". We believe that these lines act as stress-release centres during the growth of the films and are formed by diffusion and coalescence of the material which forms the grain boundaries with the driving force being the stress in the growing films. This argument is supported by the fact that the size of "islands" differs when the substrate changed. If the "network" was caused by volume shrinkage from pyrochlore to perovskite, one would expect the size of the "islands" to remain the same, irrespective of the change of the substrate.

SEM back-scattering images showed grain boundaries and line centres in PST (both CH385 and CH445) with darker contrast to grain centres. There are at least two explanations for this. One is that grain boundaries were actually holes and that there was simply less mass in the grain boundary than the grain centre. Another one is that grain boundaries were lead deficient, because lead is the most efficient of the back-scattering elements among the three elements lead, scandium and tantalum [22]. Our EDX and MBD results suggest that the latter was being the case, i.e. the grain boundary was tantalum-rich and lead-deficient compared to the grain centre. Extensive EDX results will be presented separately [17].

## 5. Conclusions

Perovskite PST thin films with and without a buffer layer of Pt/Ti/MgO on platinized silicon substrate $Pt/Ti/SiO_2/Si$ have been successfully produced at a temperature as low as 525 °C by reactive sputtering techniques. X-ray diffraction, SEM and TEM have indicated structural differences between films deposited on different substrates. It has been shown that the films without a Pt/Ti/MgO layer consisted of grains of perovskite with amorphous material at the grain boundaries, and that the perovskite grains were highly (1 1 1) preferrentially oriented. However, for PST films with a Pt/Ti/MgO layer underneath, a pyrochlore phase existed at the edge of the grain-to-grain boundaries, with perovskite at the grain centres and amorphous material at the centre of the grain boundaries. The perovskite grains were mainly (1 1 1) and (1 1 0) oriented. It is believed that these differences between the PST films were connected to the orientation differences of the platinum layers immediately under the PST. It is observed that the grain centres were perovskite whilst grain boundaries were amorphous or pyrochlore, and that the grain boundaries were tantalum-rich and lead-deficient compared to grain centres. The "lines" dividing the PST into a "network" of roughly square islands were the same as grain boundaries in terms of chemical composition and crystallography. They are believed to be formed during film growth and acted as stress-release centres in the films. The structure of platinum in Pt/Ti/MgO was believed to be influenced by the (0 0 1) textured MgO underneath it in CH445.


## Acknowledgements

This work has been carried out with the support of the Defence Research Agency (Malvern). ZH thanks Dr J. Fryer, EM Centre, University of Glasgow, for kindly allowing him to use the Topcon-002B microscope facilities there. Mr B. Diamond, Essex University, is thanked for technical help.


## References


1. R. W. WHATMORE, *Rep. Prog. Phys.* **49** (1986) 1335.
2. C. A. RANDALL, D. J. BARBER, R. W. WHATMORE and P. GROVERS, *J. Mater. Sci.* **21** (1986) 4456.
3. N. SETTER and L. E. CROSS, *ibid.* **15** (1980) 2478.
4. G. F. STENGER and A. J. BURGRAAF, *Phys. Status Solidi* (*a*) **61** (1980) 653.
5. K. Z. BABA-KISHI and D. J. BARBER, *J. Appl. Crystallogr.* **23** (1990) 43.
6. K. Z. BABA-KISHI, I. M. REANEY and D. J. BARBER, *J. Mater. Sci.* **25** (1990) 1645.
7. K. Z. BABA-KISHI, G. CRESSEY and R. J. CRENIK, *J. Appl. Crystallogr.* **25** (1992) 477.
8. C. A. RANDALL, D. J. BARBER and R. W. WHATMORE, *J. Microscop.* **145** (1987) 275.
9. N. SETTER and L. E. CROSS, *J. Appl. Phys.* **51** (1980) 4356.
10. R. WATTON, *Integr. Ferroelect.* **4** (1994) 175.
11. S. H. PYKE, K. Z. BABA-KISHI, R. WATTON and M. A. TODD, *ibid.* **4** (1994) 25.
12. C. D. MEEKISON, K. Z. BABA-KISHI, R. WATTON and M. A. TODD, *ibid.* **8** (1995) 283.
13. A. PATEL, N. SHARROCKS and R. WHATMORE, *Ferroelectrics* **134** (1992) 343.
14. D. LIU and D. PAYNE, *J. Appl. Phys.* **77** (1995) 3361.
15. C. BJORMANDER, K. SREENIVAS, A. M. GRIGHIN and K. V. RAO, *Appl. Phys. Lett.* **67** (1995) 58.
16. P. GROVES, *J. Phys. C Solid State Phys.* **18** (1985) L1073.
17. R. W. WHATMORE, Z. HUANG, M. A. TODD, *J. Appl. Phys.* (1997), in press.
18. C. HSUEH and M. McCARTNEY, *J. Mater. Res.* **6** (1991) 2208.
19. R. WATTON, *Ferroelectrics*, **184** (1996) 141.
20. K. G. BROOKS, I. M. REANEY, R. KLISSURSKA, Y. HUANG, L. BURSILL and N. SETTER, *J. Mater. Res.* **9** (1994) 2540.
21. S. HIRANO, T. YOGO, K. KIKUTA, Y. ARAKI, M. SAITOH and S. OGASAHARA, *J. Am. Ceram. Soc.* **75** (1992) 2785.
22. L. REIMER, "Scanning Electron Microscopy", edited by J. N. Chapman and A.J. Craven, (SUSSP 1983).



*Received 5 September 1996*
*and accepted 14 July 1997*